Version April 19-2016

Synthesis and Oxygen Transport Properties of $La_{2-y}Sr_yNi_{1-x}Mo_xO_{4+\delta}$

S. Y. Gómez[a,b], J. Gurauskis[a], V. Øygarden[a], D. Hotza[b], T. Grande[a] and K. Wiik[a,1]

[a] Department of Materials Science and Engineering, Norwegian University of Science and Technology (NTNU), 7491 Trondheim, Norway

[b] Departments of Chemical Engineering (EQA) and Mechanical Engineering (EMC), Federal University of Santa Catarina (UFSC), 88040-900 Florianópolis, Brazil

Abstract

$La_2NiO_{4+\delta}$-based materials (LN) with tetragonal K_2NiF_4-type structure exhibit high electronic and oxygen ion conductivity. In this work synthesis, phase relations and oxygen transport properties are reported for the system $La_{2-y}Sr_yNi_{1-x}Mo_xO_{4+\delta}$ where $0.0 \leq y \leq 0.4$ and $0.0 \leq x \leq 0.1$. The solubility of Mo in LN is low, but becomes enhanced by Sr substitution on A-site. $La_{1.8}Sr_{0.2}Ni_{0.95}Mo_{0.05}O_{4+\delta}$ (LSNM) bar shaped samples was subjected to electrical conductivity relaxation (ECR) for assessment of oxygen bulk diffusion (D_{chem}), oxygen surface exchange (k_{chem}) and electronic conductivity. The p-type conductivity was 50 $S \cdot cm^{-1}$ at 900 ºC, which is lower than both LN and LSN (Sr=0.2). On the other hand, k_{chem} was enhanced by one order of magnitude compared with LN at all temperatures, while D_{chem} was lower at T>700 ºC and higher at T<700 ºC.

Keywords: Lanthanum Nickelate, Sr- and Mo-substitution; Electrical conductivity; Oxygen diffusion; Surface exchange; Electrical Conductivity Relaxation.

[1] Corresponding author: kjell.wiik@material.ntnu.no

1. Introduction

Mixed conductors derived from nickelates with K_2NiF_4-type structure, $La_2NiO_{4+\delta}$ (LN) and doped LN-compounds have attracted much attention as promising materials for intermediate-temperature solid oxide fuel cell (IT-SOFC) cathodes and ceramic membranes for oxygen separation as well as applications involving partial oxidation of light hydrocarbons [1-9]. The advantages of LN-based materials include favorable oxygen transport properties (surface exchange and bulk diffusion) combined with moderate thermal- and chemical expansion and high electrocatalytic activity [10-13]. The K_2NiF_4-type structure of LN is tetragonal (space group I4/mmm or F4/mmm), and corresponds to alternating layers of perovskite- and rock salt structure [14-19]. The oxygen ion transport may occur by a combination of vacancy diffusion in the perovskite layer and via interstitial sites between the rock-salt and perovskite layers [18, 20, 21]. In order to estimate characteristic features of the oxygen transport and conductivity in LN based compounds, a simplified model may be considered [22-24]. As we will investigate the properties at relatively high partial pressures of oxygen we disregard the presence of oxygen vacancies and assumes that the main point defects in $La_2NiO_{4+\delta}$ are interstitial oxygen ions (O_i'') and electron holes ($h^{\bullet}$, originating from the presence of Ni^{3+}). Hence the following defect equilibria may be formulated:

$$\frac{1}{2}O_2 = O_i'' + 2\left[Ni_{Ni}^{\bullet}\right] = O_i'' + 2h^{\bullet} \qquad (1)$$

corresponding to the equilibrium constant, K_p':

$$K_p' = \frac{\left[O_i''\right]\left[h^{\bullet}\right]^2}{P_{O_2}^{\frac{1}{2}}} \qquad (2)$$

Charge balance is formulated in Eq, 3:

$$2\left[O_i''\right]=\left[h^{\cdot}\right] \quad (3)$$

And substituting Eq. 3 into Eq. 2 gives:

$$P_{O_2}^{1/2}=K_p\left[h^{\cdot}\right]^3 \quad (4)$$

where K_p is a constant. Since the electronic conductivity, σ, is proportional to the concentration of charge carriers the following proportionality should apply for the non-substituted case:

$$\sigma \propto \left[h^{\cdot}\right] \propto P_{O_2}^{\frac{1}{6}} \quad (5)$$

Substituting divalent Sr for trivalent La on A-site and hexavalent Mo for divalent Ni on B-site in $La_{2-y}A_yNi_{1-x}B_xO_{4+\delta}$, the electroneutrality may be formulated viz.:

$$2\left[O_i''\right]+\left[Sr_{La}'\right]=\left[h^{\cdot}\right]+4\left[Mo_{Ni}^{\cdots\cdot}\right] \quad (6)$$

Eqs. 1 to 6 will form the basis for discussing the behavior of conductivity for both non-substituted and substituted LN.

It is reported in the literature that substitution on B-site with a higher valent element results in a higher concentration of interstitial oxygen, which may be beneficial for the oxygen diffusivity [11, 17, 20, 21, 23-26], while incorporation of a divalent Sr on A-site suppress the oxygen diffusivity [11-13, 23]. However, doping with Sr increases the overall conductivity, and EIS studies on Sr-substituted LN show a lower area specific resistance values compared with the non-substituted compound, which is advantageous for IT-SOFC applications [27, 28].

The aim of the present work was to assess the phase relations in LN substituted with Sr and Mo and investigate the effect on electrical conductivity and oxygen transport properties (D_{chem} *and* k_{chem}) as measured by the method of electrical conductivity

relaxation (ECR).

2. Experimental

$La_{2-y}Sr_yNi_{1-x}Mo_xO_{4+\delta}$ were synthesized by two different methods, namely solid-state reaction (SS) and spray pyrolysis (SP). Precursors for the SS-synthesis were Sr-carbonate and oxides. The precursors were wet-milled (100% ethanol) in a planetary ball-mill (zirconia balls/0.5 cm) for 45 min, subsequently dried in a rotavapor prior to solid state reaction in air at temperatures between 1100 and 1500 ºC for 12 h. The SP powders were synthesized from stoichiometric aqueous solutions of La–EDTA, Ni–EDTA and Mo–malic acid solutions added dried Sr-Nitrate. Typical final concentration of solutions prior to spraying was 0.2 M. Details of spray pyrolysis procedure are given elsewhere [29]. As-prepared powders were dry ball milled for 15 min, calcined at 700 ºC for 8h, ball milled in 100% ethanol for 12 h, dried in a rotavapor and finally sieved (<50 μm). Phase composition and crystallography were assessed by X-ray diffraction (XRD: Bruker D8 Advance DaVinci) combined with Rietveld refinement for accurate determination of cell parameters.

The electrical conductivity and oxygen transport properties were measured for $La_{1.8}Sr_{0.2}Ni_{0.95}Mo_{0.05}O_{4+\delta}$ and assessed by electrical conductivity relaxation (ECR) with a four-point DC method at temperatures between 600 and 900 ºC using bar samples [30]. The bar-shaped green bodies (based on spray pyrolysed powder) were prepared by uniaxial pressing (0.8kN) followed by cold isostatic pressing (CIP, 200MPa). The green bodies were sintered in air at 1500 ºC for 4 h. The density was measured by the Archimedes´ method and the microstructure (fracture and polished surface) and element mapping (polished surface) was analyzed by scanning electron microscopy combined

with energy dispersive spectroscopy (SEM/EDS: Hitachi S-3400N). The sintered bars were cut, grinded and finally polished (1 μm diamond paste) to final dimensions of 1×5×20 mm. A N_2/O_2 gas-mixing equipment (5.0 purity both gases) was used to control the oxygen partial pressure, which was varied stepwise between 0.2 and 0.0066 atm. Each step corresponded to 1/4-order of magnitude ($\log(\Delta P_{O_2}) = 0.25$). A small step in oxygen partial pressure will increase the accuracy of the oxygen transport coefficients according to recommendations given in [30]. Both oxidation and reduction steps were performed.

The transient conductivity relaxation behavior can be precisely described by Fick's second law [31]:

$$\frac{\sigma_t - \sigma_t}{\sigma_\infty - \sigma_0} = 1 - \sum_{n=1}^{\infty} \frac{2A^2 \exp(-\beta_n^2 D_{chem} t / l^2)}{\beta_n^2 (\beta_n^2 + A^2 + A)} \qquad (7)$$

where σ_0, σ_t, and σ_∞ denote the conductivity at the initial time, t, and infinite time, respectively. D_{chem} is the chemical diffusion coefficient of oxygen. A is a measure of the contribution from the surface exchange defined as the ratio of half the sample thickness l to the characteristic length l_d as:

$$A = \frac{l}{l_d} = \frac{l \times k_{chem}}{D_{chem}} \qquad (8)$$

where k_{chem} is the surface exchange coefficient and β_n is the positive root of:

$$\beta_n \tan \beta_n = A \qquad (9)$$

Eq. 7 can be solved numerically and further details are given elsewhere [30, 32]. D_{chem} and k_{chem} were determined by fitting of the electrical conductivity relaxation data.

3. Results and Discussion

3.1. Phase Relations

XRD-analysis of LN substituted with Mo is shown in Fig. 1. Formation of secondary phases is evident for a Mo-content $x \geq 0.0125$. Assuming that equilibrium is established, a perovskite type phase ($LaMo_{0.2}Ni_{0.8}O_3$) coexists with the main LN-phase for x(Mo)=0.0125 and 0.025, while three phases coexist at x(Mo)=0.05 ($LaMo_{0.2}Ni_{0.8}O_3$, La_6MoO_{12} and the main LN phase).

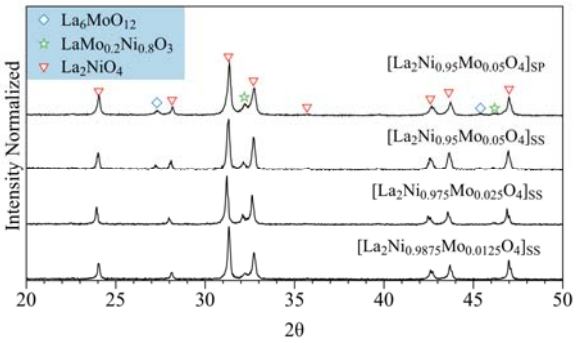

Figure 1. Diffractograms of $La_2Ni_{1-x}Mo_xO_{4+\delta}$ with x=0.0125, 0.025, 0.05. All SS-samples are sintered at 1300°C while SP-sample is sintered at 1400°C. The presence of the major phase is compared with the characteristic reflections for tetragonal La_2NiO_4.

$La_{1.8}Sr_{0.2}Ni_{0.95}Mo_{0.05}O_{4+\delta}$ sintered at temperatures between 1250 and 1500 ºC was single phase, inferring that the solid solubility of Mo $x \leq 0.05$ at Sr-content y=0.2. XRD-analysis of the corresponding samples with higher Mo-contents is displayed in Fig. 2 and disclose the presence of a secondary phase (perovskite type) at x>0.05. $La_{1.6}Sr_{0.4}Ni_{0.95}Mo_{0.05}O_{4+\delta}$ was also prepared, but no phase pure samples could be obtained due to the formation of the secondary phase $SrMoO_4$. A summary of phase relations for all compositions are given in Table 1.

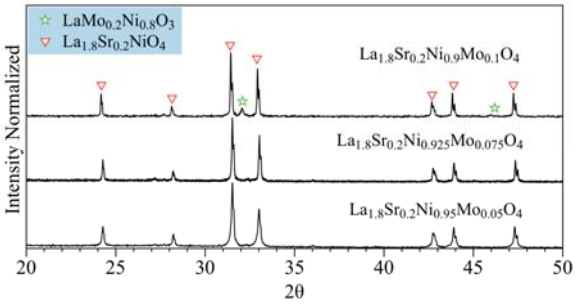

Figure 2. XRD-data for $La_{1.8}Sr_{0.2}Ni_{1-x}Mo_xO_{4+\delta}$ (SS-samples) with x=0.05, 0.075 and 0.1. All samples are sintered at 1300 ºC. The major LN phase is compared with the characteristic reflections for $La_{1.8}Sr_{0.2}NiO_4$.

Table 1. Synthesis methods, sintering temperature and phases observed according to XRD-analysis for the nominal stoichiometry: $La_{2-y}Sr_yNi_{1-x}Mo_xO_{4+\delta}$. Cell parameters obtained by Rietveld refinement for the major LN phase are also listed. Estimated errors in cell parameters are ±0.0015 Å and ±0.003 Å for a- and c-axis, respectively.

y	x	Method	T/ºC	Major Phase	Minor Phases	a (Å)	c (Å)
0.0	0.05	SP	1400	$La_2Ni_{1-z}Mo_zO_{4+\delta}$	La_6MoO_{12} - $LaMo_{0.2}Ni_{0.8}O_3$	3.866	12.665
	0.0125	SS	1300	$La_2Ni_{1-z}Mo_zO_{4+\delta}$	$LaMo_{0.2}Ni_{0.8}O_3$	3.864	12.679
	0.025	SS	1300	$La_2Ni_{1-z}Mo_zO_{4+\delta}$	$LaMo_{0.2}Ni_{0.8}O_3$	3.863	12.682
	0.05	SS	1300	$La_2Ni_{1-z}Mo_zO_{4+\delta}$	La_6MoO_{12}- $LaMo_{0.2}Ni_{0.8}O_3$	3.863	12.676
0.2	0.05	SP	1250	$La_{1.8}Sr_{0.2}Ni_{0.95}Mo_{0.05}O_{4+\delta}$	-	3.848	12.695
	0.05	SP	1400	$La_{1.8}Sr_{0.2}Ni_{0.95}Mo_{0.05}O_{4+\delta}$	-	3.848	12.676
	0.05	SP	1500	$La_{1.8}Sr_{0.2}Ni_{0.95}Mo_{0.05}O_{4+\delta}$	-	3.849	12.675
	0.05	SS	1300	$La_{1.8}Sr_{0.2}Ni_{0.95}Mo_{0.05}O_{4+\delta}$	-	3.847	12.696
	0.075	SS	1300	$La_{1.8}Sr_{0.2}Ni_{1-z}Mo_zO_{4+\delta}$	$LaMo_{0.2}Ni_{0.8}O_3$	3.847	12.688
	0.1	SS	1300	$La_{1.8}Sr_{0.2}Ni_{1-z}Mo_zO_{4+\delta}$	$LaMo_{0.2}Ni_{0.8}O_3$	3.847	12.689
0.4	0.05	SP	1400	$La_{1.6}Sr_{0.4}Ni_{1-z}Mo_zO_{4+\delta}$	$SrMoO_4$	3.287	12.704
	0.05	SP	1500	$La_{1.6}Sr_{0.4}Ni_{1-z}Mo_zO_{4+\delta}$	$SrMoO_4$	3.830	12.702
	0.05	SS	1100	$La_{1.6}Sr_{0.4}Ni_{1-z}Mo_zO_{4+\delta}$	$SrMoO_4$	3.827	12.711
	0.05	SS	1200	$La_{1.6}Sr_{0.4}Ni_{1-z}Mo_zO_{4+\delta}$	$SrMoO_4$	3.826	12.708
	0.05	SS	1300	$La_{1.6}Sr_{0.4}Ni_{1-z}Mo_zO_{4+\delta}$	$SrMoO_4$	3.828	12.705
	0.05	SS	1400	$La_{1.6}Sr_{0.4}Ni_{1-z}Mo_zO_{4+\delta}$	$SrMo_4$	3.830	12.703

The K_2NiF_4-type structure of $La_{2-y}Sr_yNi_{1-x}Mo_xO_{4+\delta}$ was found to be tetragonal with space group I4/mmm. Fig. 3 shows the variation in the a- and c- axis with Mo-substitution for compositions with Sr-content corresponding to y=0, 0.2 and 0.4. Both a and c change with Sr-substitution, While a contracts with Sr-substitution c expands. The first can be explained by oxidation of Ni due to Sr-substitution, while the second can be rationalized by the larger ionic size of Sr^{2+} relative to La^{3+}. The a-parameter is relatively insensitive to Mo-substitution, while c clearly expand due to Mo-substitution

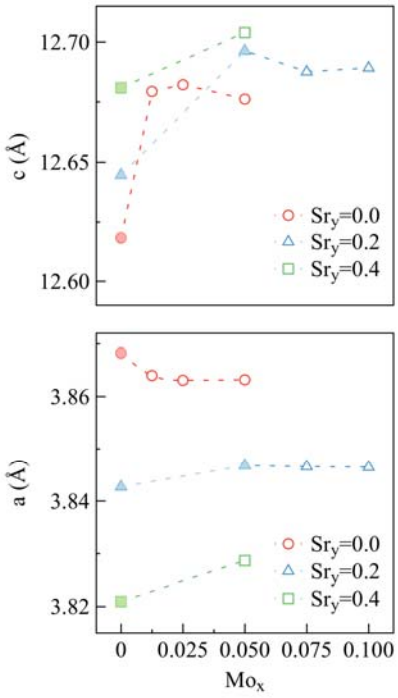

Figure 3. Variation in cell parameter for $La_{2-y}Sr_yNi_{1-x}Mo_xO_{4+\delta}$ with Mo-content for compositions with 0.0, 0.2 and 0.4 Sr. Cell parameters for La_2NiO_4 is taken from [14]. Samples are heat treated at T=1300^{o}C. Open symbols indicate single phase while filled symbols indicate the presence of secondary phases. Magnitude of error will typically be within the size of the symbols given in the figures.

A comparison among lattice parameters is given in Fig. 4. The c-axis expands as B-site is substituted with 10% Co and 10% Fe, while the a-axis is virtually independent. However, for compositions with Sr content x=0.2, the c-axis expands significantly and a-axis moderately as 0.05 Mo is added. Assuming 6-valent Mo on B-site, the expanded lattice may be due to an overall increase in interstitial oxygen. The ionic radius of 6-valent Mo (6-coordinated, 0.59 Å) is significantly smaller than divalent Ni (6-coordinated, 0.69 Å) and should not result in expansion based on size only. These assumptions are based on a dominating presence of divalent Ni on B-site, at conditions where a significant fraction of Ni is oxidized to trivalent Ni the ionic radii of Mo^{6+} and Ni^{3+} (high spin, 6-coordinated, 0.6 Å) are similar and substitution with Mo should not contribute to changes in unit cell based on ionic radii only.

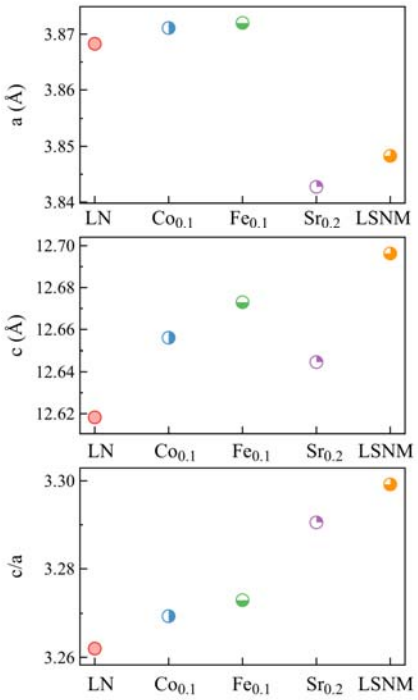

Figure 4. Comparing lattice parameters for LN [14] and LN substituted with Co=0.1 [20], Fe=0.1 [11] and Sr=0.2 [14]. Sample substituted with both Sr and Mo (LSNM) is taken from this work.

3.2. Conductivity and Oxygen Transport Properties

Single phase $La_{1.8}Sr_{0.2}Ni_{0.95}Mo_{0.05}O_{4+\delta}$ (SP-powder) were sintered in air at 1500 ^{o}C for 4 hours. Density was found to be 6.645 g/cm^3 corresponding to > 95% dense as compared with a theoretical density of 6.929 g/cm^3 (based on XRD-data). The resulting grain size showed a rather large variation (Fig. 12) corresponding to 14±8 µm. The bars of $La_{1.8}Sr_{0.2}Ni_{0.95}Mo_{0.05}O_{4+\delta}$ were subjected to ECR to assess both oxygen transport properties and electrical conductivity as a function of temperature and partial pressure oxygen. Typical ECR-curves are given in Fig. 5, for both oxidation- and reduction step. The results presented in this section are based on one sample only.

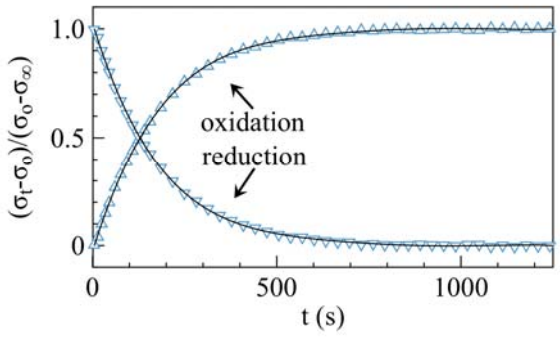

Figure 5. Typical electrical conductivity relaxation (ECR) profile of $La_{1.8}Sr_{0.2}Ni_{0.95}Mo_{0.05}O_{4+\delta}$ at 700 ºC. Oxidation and reduction steps corresponding to 0.066-0.1175 atm and 0.2-0.1175 atm, respectively. The blue triangles represent measured values while the solid lines show the results of fitting experimental data according to Eq. 7.

The oxygen pressure and temperature dependencies of the electrical conductivity for $La_{1.8}Sr_{0.2}Ni_{0.95}Mo_{0.05}O_{4+\delta}$ compared with LN and LSN are shown in Figs. 6-7. The conductivity for all materials is seen to increase linearly with pO_2 consistent with p-type conductivity, Eq. 5. Adding Sr to LN gives a significant increase in conductivity while the presence of Mo reduces the conductivity even below LN. According to the relationship given in Eq. 5, a 1/6-slope is predicted for LN, this behavior is reported by Jeon et al. [34] at low pO_2´s, however, at higher partial pressures they report a less pronounced dependency approaching 1/10. The reason for the deviation at higher pO_2´s may be due to formation of clusters and associates of point defects forming neutral point defects [35]. A defect model taking these phenomena into account is beyond the scope of the present work. It is evident from Figs. 6-7 that Mo reduce the electronic conductivity to some degree, the reasons for this may be twofold: The p-type conductivity is governed by a polaron hopping mechanism corresponding to electrons jumping between Ni-sites. 6- valent Mo- will occupy a Ni- site as $Mo_{Ni}^{\bullet\bullet\bullet\bullet}$ (Cf. Eq. 6), and may block the pathway for electronic charge carriers. Secondly, Mo may also reduce the average oxidation number of Ni corresponding to a lower fraction of Ni^{3+}/Ni^{2+}, that is, reduce the concentration of holes ($h^{\bullet}$). This may be elaborated further, assuming the presence of 0.05 $Mo_{Ni}^{\bullet\bullet\bullet\bullet}$ on Ni-site it is interesting to notice that this will be exactly charge compensated by 0.2 Sr_{La}' on La-site, indicating that the negative charge due to Sr-substitution is compensated by $Mo_{Ni}^{\bullet\bullet\bullet\bullet}$ rather than the formation of holes, $h^{\bullet}$. The overall effect will be a reduced electronic conductivity.

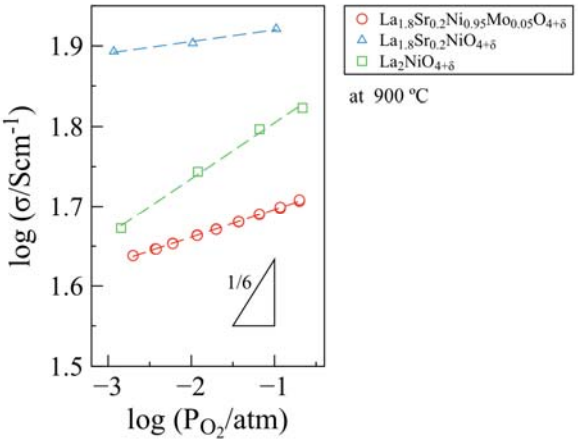

Figure 6. Conductivity vs. P_{O2} at 900 ºC for LN [34], LN substituted with Sr=0.2 [28] and $La_{1.8}Sr_{0.2}Ni_{0.95}Mo_{0.05}O_4$.

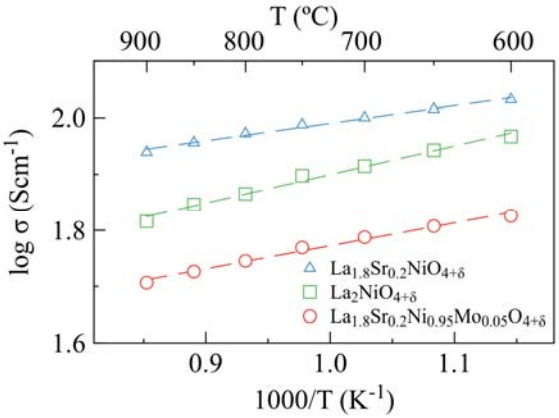

Figure 7. Conductivity of $La_{1.8}Sr_{0.2}Ni_{0.95}Mo_{0.05}O_{4+\delta}$ vs. temperature in air compared with LN and LSN [28].

The oxygen transport properties resulting from ECR-analysis are given in Figs. 8-10. It is seen in Fig. 8 that k_{chem} is only marginally higher for a reduction step compared with an oxidation step, while D_{chem} is virtually independent of the type of step. Both D_{chem} and k_{chem} increase with pO_2 and temperature. In Fig. 9 the temperature dependency of D_{chem} for LSNM is compared with LN and LSN reported in the literature. The D_{chem} are average values from oxidation and reduction steps. The activation energies for LSN and

LSNM are rather similar, and adding Mo on B-site significantly increase the bulk-diffusion coefficient, probably due to increased population of mobile interstitial oxygen corresponding to substitution of divalent Ni with 6-valent Mo (Eq. 6). The activation energy for LN is about twice the activation energy observed for LSN and LSNM. At temperatures < 700 °C D_{chem} for LSNM is higher than D_{chem} for LN, hence substitution with Mo may give an advantage with respect to bulk diffusion at moderate temperatures.

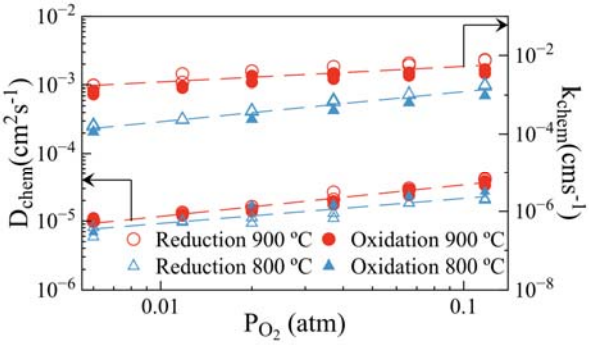

Figure 8. D_{chem} and k_{chem} vs. Po_2 for $La_{1.8}Sr_{0.2}Ni_{0.95}Mo_{0.05}O_{4+\delta}$ at 800 and 900 ºC assessed by ECR. pO_2-step is 1/4-order of magnitude both for oxidation and reduction.

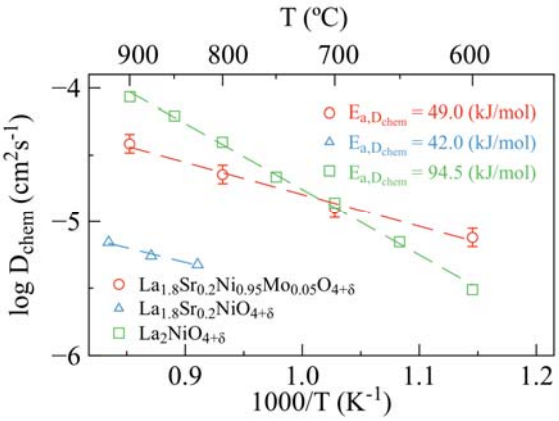

Figure 9. Plot of D_{chem} vs. temperature and activation energies for $La_{1.8}Sr_{0.2}Ni_{0.95}Mo_{0.05}O_{4+\delta}$ (pO_2-step=0.2 to 0.117 atm), compared with $La_{1.8}Sr_{0.2}NiO_{4+\delta}$ [36] (Po_2-step=0.066 to 0.2 atm) and $La_2NiO_{4+\delta}$ [37] (Po_2-step=1.0 to 0.2 atm).

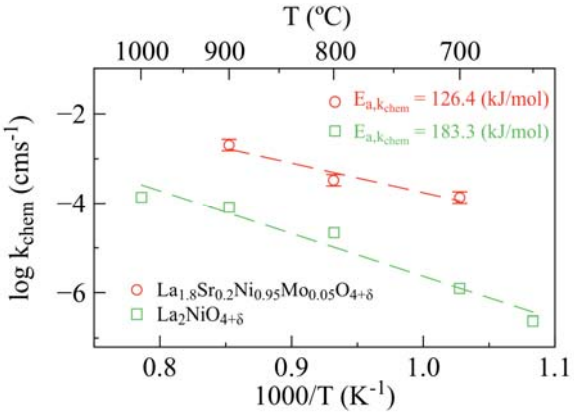

Figure 10. k_{chem} vs. temperature and activation energies for LSNM (Po_2-step=0.037 to 0.02 atm) and LN [34] (Po_2-step =0.066 to 0.02 atm).

Surface exchange coefficients (k_{chem}) vs. temperature compared with LN and LSN are summarized in Fig. 10. It is seen that surface exchange is enhanced with more than one order of magnitude when LN is substituted with a combination of Sr (0.2) and Mo (0.05**)**. This gives promise from an application point of view, being able to produce membranes with thickness less than the critical thickness rather high oxygen permeation fluxes may be obtained.

XRD-analysis of samples before and after ECR is given in Fig. 11. Whereas the surface is single phase according to XRD prior to test, traces of a secondary phase is observed at the surface after ECR. Although XRD-analysis do not indicate secondary phases at the surface before ECR, SEM-images give in Fig. 12 a-b show the presence of a few grains apparently sticking out of the surface. This may indicate that the solubility limit for Mo in $La_{1.8}Sr_{0.2}Ni_{1-x}Mo_xO_{4+\delta}$ –has been reached and a secondary Mo-rich phase has been formed, implicating that the solubility of Mo in $La_{1.8}Sr_{0.2}Ni_{1-x}Mo_xO_{4+\delta}$ is slightly less than x=0.05. XRD-surface analysis after ECR clearly shows the presence of a

secondary phase, probably corresponding to the small grains peeking out of the surface as shown in the SEM-image in Fig. 12c. In the backscatter image (Fig. 12d) these grains appear black possibly due to topography. EDS-analysis of surface after ECR is given in Fig. 13 and shows areas enriched with Sr and Mo, which may be due to the formation of $SrMoO_4$. Nevertheless, XRD- and SEM-analysis of the bulk phase after ECR (Fig. 11 and Fig. 12e-f) indicate absence of secondary phases, or at least below the detection limit. The transport coefficients resulting from ECR-analysis did not change during 3-weeks of testing at elevated temperatures, indicating that eventual formation of secondary phases at the surface did not affect the oxygen transport properties in the time interval investigated.

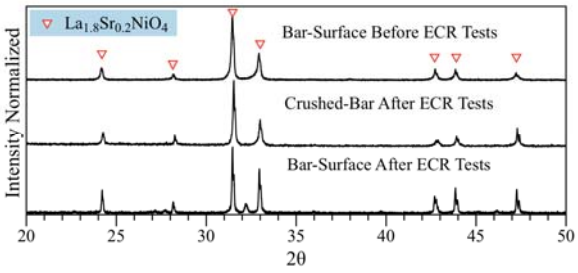

Figure 11. XRD-analysis of $La_{1.8}Sr_{0.2}Ni_{0.95}Mo_{0.05}O_{4+\delta}$ –samples before and after the electrical conductivity relaxation (ECR) tests. Upper and lower curve show surface analysis, while the curve in between is representative for the bulk (crushed sample) after ECR.

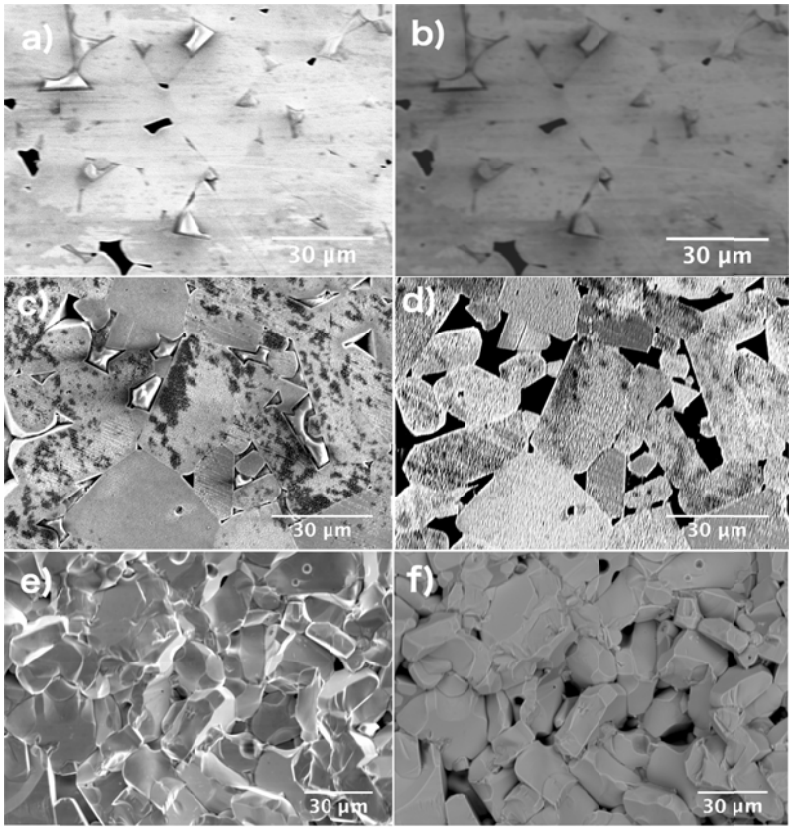

Figure 12. SEM of bar-shaped samples before ECR: a) polished surface (secondary electrons), b) polished surface (backscatter secondary electrons). After ECR: c) polished surface (secondary electrons), d) polished surface (backscatter secondary electrons), e) fracture surface (secondary electrons), f) fracture surface (backscatter secondary electrons).

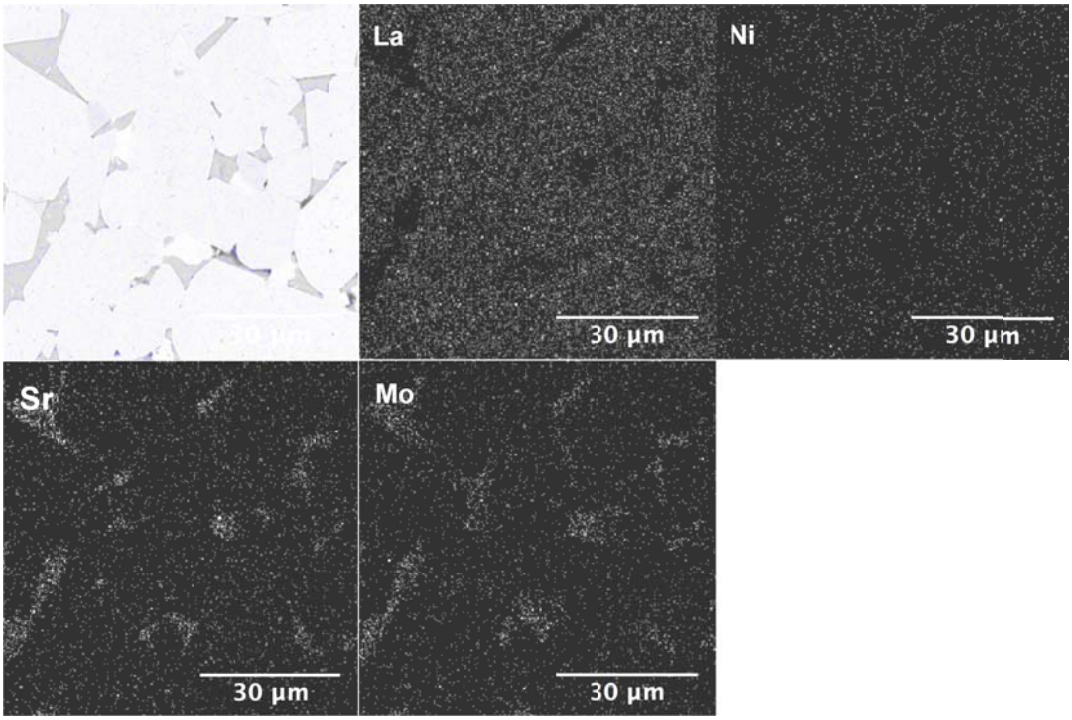

Figure 13. EDS analysis of polished surface after ECR.

4. Conclusion

Phase relations have been established for the system $La_{2-y}Sr_yNi_{1-x}Mo_xO_{4+\delta}$ where $0.0 \leq y \leq 0.4$ and $0.0 \leq x \leq 0.1$. For all materials the main phase (K_2NiF_4-type) showed tetragonal symmetry. The solubility of Mo in LN is low, but is enhanced by Sr substitution on A-site. The c-axis was found to expand significantly both with Sr- and Mo-substitution, while contraction of the a-axis was observed with Sr-substitution. The a-axis was less dependent on Mo-substitution. The variation in cell parameters was interpreted by a combination of ratios between the various ionic radii and interstitial oxygen. The solubility limit for Mo in LN was established at $Mo \approx 0.0125$ and 1300 ºC while substitution with Sr (x=0.2) increased the solubility limit to $Mo \approx 0.05$ at the same temperature. The electronic p-type conductivity of $La_{1.8}Sr_{0.2}Ni_{0.95}Mo_{0.05}O_{4+\delta}$ (LSNM) was ~50 $S \cdot cm^{-1}$ at 900 ºC, which is lower than both LN and LSN (Sr=0.2). However,

k_{chem} was enhanced by one order of magnitude compared with LN at all temperatures while D_{chem} showed lower values at T>700 ºC and higher at T<700 ºC. Most likely $SrMoO_4$ was observed on the surface after conductivity measurements, but the presence of the secondary phase did not affect the oxygen transport properties.

Acknowledgements

This work was supported by The Research Council of Norway (NFR) – Yggdrasil mobility program (219786/F11).

References

[1] Mauvy F, Lalanne C, Bassat J-M, Grenier J-C, Zhao H, Huo L, et al. Electrode properties of Ln2NiO4 + δ (Ln = La , Nd , Pr) : AC Impedance and DC Polarization Studies. J Electrochem Soc. 2006;153:A1547-A53.

[2] Dailly J, Fourcade S, Largeteau A, Mauvy F, Grenier JC, Marrony M. Perovskite and A(2)MO(4)-type oxides as new cathode materials for protonic solid oxide fuel cells. Electrochim Acta. 2010;55:5847-53.

[3] Boehm E, Bassat JM, Dordor P, Mauvy F, Grenier JC, Stevens P. Oxygen diffusion and transport properties in non-stoichiometric Ln2−xNiO4+δ oxides. Solid State Ionics. 2005;176:2717-25.

[4] Sayers R, Liu J, Rustumji B, Skinner SJ. Novel K2NiF4-Type Materials for Solid Oxide Fuel Cells: Compatibility with Electrolytes in the Intermediate Temperature Range. Fuel Cells. 2008;8:338-43.

[5] Montenegro-Hernández A, Vega-Castillo J, Mogni L, Caneiro A. Thermal stability of Ln2NiO4+δ (Ln: La, Pr, Nd) and their chemical compatibility with YSZ and CGO solid electrolytes. Int J Hydrogen Energ. 2011;36:15704-14.

[6] Laguna-Bercero MA, Hanifi AR, Monzon H, Cunningham J, Etsell TH, Sarkar P. High performance of microtubular solid oxide fuel cells using Nd2NiO4+ δ -based composite cathodes. Journal of Materials Chemistry A. 2014;2:9764-70.

[7] Zhao K, Wang Y-P, Chen M, Xu Q, Kim B-H, Huang D-P. Electrochemical evaluation of La2NiO4+δ as a cathode material for intermediate temperature solid oxide fuel cells. Int J Hydrogen Energ. 2014;39:7120-30.

[8] Zhang X, Zhang H, Liu X. High performance La2NiO4+δ-infiltrated (La0.6Sr0.4)0.995Co0.2Fe0.8O3−δ cathode for solid oxide fuel cells. J Power Sources. 2014;269:412-7.

[9] Kharton VV, Yaremchenko AA, Valente AA, Sobyanin VA, Belyaev VD, Semin GL, et al. Methane oxidation over Fe-, Co-, Ni- and V-containing mixed conductors. Solid State Ionics. 2005;176:781-91.

[10] Al Daroukh M, Vashook VV, Ullmann H, Tietz F, Arual Raj I. Oxides of the AMO3 and A2MO4-type: structural stability, electrical conductivity and thermal expansion. Solid State Ionics. 2003;158:141-50.

[11] V. Kharton V, P. Viskup A, N. Naumovich E, M. B. Marques F. Oxygen ion transport in La2NiO4-based ceramics. J Mater Chem. 1999;9:2623-9.

[12] Skinner SJ, Kilner JA. A comparison of the transport properties of La2−xSrxNi1−yFeyO4+δ where 0<x<0.2 and 0<y<0.2. Ionics. 1999;5:171-4.

[13] Skinner SJ, Kilner JA. Oxygen diffusion and surface exchange in La2−xSrxNiO4+δ. Solid State Ionics. 2000;135:709-12.

[14] Takeda Y, Kanno R, Sakano M, Yamamoto O, Takano M, Bando Y, et al. Crystal chemistry and physical properties of La2−xSrxNiO4 ($0 \leq x \leq 1.6$). Mater Res Bull. 1990;25:293-306.

[15] Singh KK, Ganguly P, Goodenough JB. Unusual effects of anisotropic bonding in Cu(II) and Ni(II) oxides with K2NiF4 structure. J Solid State Chem. 1984;52:254-73.

[16] James M, Attfield JP. Synthesis, crystal structure and magnetic properties of Ln2-SrNiO4 +/- δ solid solutions (Ln = La, Nd, Sm and Gd; $1.0 \leq x \leq 1.67$). J Mater Chem. 1996;6:57-62.

[17] Tsipis EV, Naumovich EN, Patrakeev MV, Waerenborgh JC, Pivak YV, Gaczyński P, et al. Oxygen non-stoichiometry and defect thermodynamics in La2Ni0.9Fe0.1O4+δ. Journal of Physics and Chemistry of Solids. 2007;68:1443-55.

[18] Tarancon A, Burriel M, Santiso J, Skinner SJ, Kilner JA. Advances in layered oxide cathodes for intermediate temperature solid oxide fuel cells. J Mater Chem. 2010;20:3799-813.

[19] Aguadero A, Escudero MJ, Perez M, Alonso JA, Pomjakushin V, Daza L. Effect of Sr content on the crystal structure and electrical properties of the system La2-SrNiO4+δ ($0 \leq x \leq 1$). Dalton Transactions. 2006:4377-83.

[20] Yaremchenko AA, Kharton VV, Patrakeev MV, Frade JR. p-Type electronic conductivity, oxygen permeability and stability of La2Ni0.9Co0.1O4+ δ. J Mater Chem. 2003;13:1136-44.

[21] Kharton VV, Tsipis EV, Naumovich EN, Thursfield A, Patrakeev MV, Kolotygin VA, et al. Mixed conductivity, oxygen permeability and redox behavior of K2NiF4-type La2Ni0.9Fe0.1O4+δ. J Solid State Chem. 2008;181:1425-33.

[22] Li Z, Haugsrud R, Smith JB, Norby T. Transport properties and defect analysis of La1.9Sr0.1NiO4+δ. Solid State Ionics. 2009;180:1433-41.

[23] Kharton VV, Viskup AP, Kovalevsky AV, Naumovich EN, Marques FMB. Ionic transport in oxygen-hyperstoichiometric phases with K2NiF4-type structure. Solid State Ionics. 2001;143:337-53.

[24] Jeon S-Y, Singh B, Im H-N, Seong K-P, Song S-J. Charge and mass transport properties of La2Ni0.95Al0.05O4.025+δ. J Alloy Compd. 2014;589:572-8.

[25] Munnings CN, Skinner SJ, Amow G, Whitfield PS, Davidson IJ. Oxygen transport in the La2Ni1−xCoxO4+δ system. Solid State Ionics. 2005;176:1895-901.

[26] Kilner JA, Shaw CKM. Mass transport in La2Ni1−xCoxO4+δ oxides with the K2NiF4 structure. Solid State Ionics. 2002;154–155:523-7.

[27] Kammer K. An EIS study of La2 − x Sr x NiO4 + δ SOFC cathodes. Ionics. 2009;15:325-8.

[28] Nakamura T, Yashiro K, Sato K, Mizusaki J. Electronic state of oxygen nonstoichiometric La2-xSrxNiO4+ δ at high temperatures. Physical Chemistry Chemical Physics. 2009;11:3055-62.

[29] Mokkelbost T, Andersen Ø, Strøm RA, Wiik K, Grande T, Einarsrud M-A. High-Temperature Proton-Conducting LaNbO4-Based Materials: Powder Synthesis by Spray Pyrolysis. J Am Ceram Soc. 2007;90:3395-400.

[30] Lohne ØF, Søgaard M, Wiik K. The Significance of Gas-Phase Mass Transport in Assessment of kchem and Dchem. J Electrochem Soc. 2013;160:F1282-F92.

[31] Crank J. The mathematics of diffusion / by J. Crank. Oxford [England]: Clarendon Press; 1975.

[32] den Otter MW, van der Haar LM, Bouwmeester HJM. Numerical evaluation of eigenvalues of the sheet diffusion problem in the surface/diffusion mixed regime. Solid State Ionics. 2000;134:259-64.

[33] Gopalakrishnan J, Colsmann G, Reuter B. Studies on the La2−xSrxNiO4 ($0 \leqslant x \leqslant 1$) system. J Solid State Chem. 1977;22:145-9.

[34] Jeon S-Y, Choi M-B, Hwang J-H, Wachsman ED, Song S-J. Electrical Conductivity and Thermoelectric Power of La2NiO4+δ. J Electrochem Soc. 2011;158:B476-B80.

[35] Vashook VV, Yushkevich II, Kokhanovsky LV, Makhnach LV, Tolochko SP, Kononyuk IF, et al. Composition and conductivity of some nickelates. Solid State Ionics. 1999;119:23-30.

[36] Syvertsen GE, Wiik K. Student project. DMSE. Trondheim, Norway: Norwegian University of Science and Technology - NTNU; 2011.

[37] Li Z, Haugsrud R. Effects of surface coatings on the determination of Dchem and kchem in La2NiO4+δ by conductivity relaxation. Solid State Ionics. 2012;206:67-71.